HOSTED BY

ELSEVIER

CrossMark

Available online at www.sciencedirect.com

ScienceDirect

Progress in Natural Science: Materials International 26 (2016) 85–89

Progress in Natural Science Materials International

www.elsevier.com/locate/pnsmi
www.sciencedirect.com

Original Research

Interfacial behavior of $Fe_{76}Si_9B_{10}P_5/Zn_{0.5}Ni_{0.5}Fe_2O_4$ amorphous soft magnetic composite during spark plasma sintering process

Zhankui Zhao*, Yueting Sun, Minggang Wang, Yue Chi, Hongli Wang

Key Laboratory of Advanced Structural Materials, Ministry of Education, Changchun University of Technology, Changchun 130012, China

Received 20 July 2015; accepted 11 November 2015
Available online 17 February 2016

Abstract

$Fe_{76}Si_9B_{10}P_5/Zn_{0.5}Ni_{0.5}Fe_2O_4$ amorphous composite with micro-cellular structure and high electrical resistivity was prepared by spark plasma sintering (SPS) at 487 °C. XRD and SEM results showed that the $Fe_{76}Si_9B_{10}P_5$ alloy powders remained the amorphous state and the composite was dense. A fusion zone at interface of $Fe_{76}Si_9B_{10}P_5$ cell body and $Zn_{0.5}Ni_{0.5}Fe_2O_4$ cell wall was observed by TEM, which also indicates the formation of local high temperature. The interface bonding based on the formation of local high temperature in SPS process was observed. It is believed that the tip effect of $Zn_{0.5}Ni_{0.5}Fe_2O_4$ nanoparticles promotes the local discharging and plasmas creation in the gaps, and the discharging energy forms an instantaneous local high temperature to complete the local sintering and the densification of $Zn_{0.5}Ni_{0.5}Fe_2O_4$ particles at a low nominal sinter temperature. Simultaneously, the local high temperature stimulates the adjacent gaps discharging, thus facilitate the continuous formation of new discharging path. Finally, sintering and densification of the amorphous composite is complete.

Keywords: Amorphous soft magnetic composite; Spark plasma sintering; Interfacial behavior

1. Introduction

Amorphous alloys are of great interest with many advantages: high mechanical strength, high hardness, good fracture toughness, low dimension, etc [1]. Amorphous magnetic materials also have excellent soft magnetic properties [2], bulk $Fe_{76}Si_9B_{10}P_5$ amorphous alloy has high saturation magnetic flux density, $Bs=1.51$ T, $Hc=0.8$ A/m, and also with high amorphous forming ability [3,4]. Generally, larger size amorphous alloys are obtained by powder metallurgy (PM) method [5]. Spark plasma sintering (SPS) is a remarkable method for synthesizing materials with many advantages: low sintering temperature and rapid sintering, etc [6]. SPS technology can avoid crystallization and has been used to prepare many amorphous metals with larger size, such as Ti–Zr–Cu–Pd–Sn [7], Zr–Cu–Al–Ni [8], Fe–B–Nd–Y [9] and Al–Cu–Ti [10].

T. Hirai [11,12] performed in-situ monitoring in SPS and found that the sintering process is absolutely different in conductive and non-conductive materials: Joule heating and pulse discharging are the main mechanism in conductive powders; while for non-conductive powders, heat conduction from the die is the major mechanism. It has also been reported that there was apparent temperature difference from the sample border to the core, especially for non-conductive materials [13,14]. In our previous study, we prepared $Al_{90}Mn_9Ce_1/Al_2O_3$ micro-cellular composite by SPS at 520 °C, above-mentioned SPS mechanism of conductive and non-conductive powders cannot explain "low temperature sintering phenomenon" of the micro-cellular composite, we proposed the sintering mechanism of instantaneous local high temperature of the interface, and we assumed the main effect promoted by the excellent SPS process to be as follows: microscopic local discharging and the activation effect by the spark plasmas stimulated the generation of an instantaneous high temperature [15]. However, there was not enough evidence to support this opinion.

*Corresponding author. Tel./fax: +86 431 85716644.
E-mail address: zhaozk@ccut.edu.cn (Z. Zhao).
Peer review under responsibility of Chinese Materials Research Society.

http://dx.doi.org/10.1016/j.pnsc.2016.01.015

In this paper, we prepared the $Fe_{76}Si_9B_{10}P_5/Zn_{0.5}Ni_{0.5}Fe_2O_4$ amorphous composite with a micro-cellular structure by SPS based on "micro-cellular sintering mechanism" [15], and investigated the interface composition and structure of the composite, to confirm the SPS mechanism of micro-cellular composite based on the formation of instantaneous local high temperature.

2. Materials and methods

Pure iron powders (99.98 wt%), pre-melted Fe-P (99.9 wt-%), pure nonmetallic crystalline powders B (99.5 wt%) and Si (99.999 wt%) were used as the raw materials. The alloy composition represents nominal atomic percentage. The $Zn_{0.5}Ni_{0.5}Fe_2O_4$ nano-powders have a purity of 99.8% and an average particle diameter of 20 nm, supplied by Deke New Materials Co. Ltd. The $Fe_{76}Si_9B_{10}P_5$ powders were prepared by gas-atomization method with above-mentioned raw materials in an argon atmosphere. The preparation parameters were as following: jet diameter of 0.8 mm, melting temperature of 1200 °C, jet pressure of 9.3 MPa. Then the obtained $Fe_{76}Si_9B_{10}P_5$ powders were sieved until the particle size was 25–45 μm, and mixed with $Zn_{0.5}Ni_{0.5}Fe_2O_4$ powders in an agate mortar milling for 25 min, with weight ratio of 9:1. Subsequently, the milled powders were pre-compacted and then sintered in Dr. SINTER. SPS-625 (pulse current on: off = 12:2) to obtain the compacts, and the sintering parameters were as follows: heating rate of 100 °C/min, pressure of 500 MPa, without holding time, sintering temperature of 467 °C, 487 °C, 507 °C, and 527 °C, respectively. Kentanium dies were used in this process, and the hole in the die was used to measure the temperature by a thermoelectric couple. The sintered samples were cylindrical with the dimension of Φ 15 mm × 3 mm.

The structures were characterized by X-ray diffraction (Modle D/MAX-2000/PC in Cu radiation), and microstructures of the powders and bulk composite were observed by SUPRA 40 field emission scanning electron microscopy (FESEM). Further observation was carried out on a JEM2010F transmission electron microscope (TEM).

3. Results

Fig. 1 shows the XRD patterns of the samples at different sintering temperature, the samples were still amorphous without any crystallization phase when T = 467 °C, 487 °C. When T = 507 °C, there appears crystallization, but not very remarkable. The crystallization is remarkable when T = 527 °C, and the main precipitated phases were: α-Fe, Fe_3B, Fe_2B, this depicts higher sintering temperature promotes crystallization of $Fe_{76}Si_9B_{10}P_5$. Besides, as Lu's study, on the basis of free volume model, pressure has an influence on the glass transition temperature (T_g) of amorphous materials: T_g will decrease by 30 K when the shear stress is 500 MPa [16], so higher pressure will promote the crystallization process at higher sintering temperature. The theoretical glass transition temperature T_g and the crystallization temperature T_x of $Fe_{76}Si_9B_{10}P_5$ alloy are 507 °C and 557 °C [4], respectively, and the crystallization

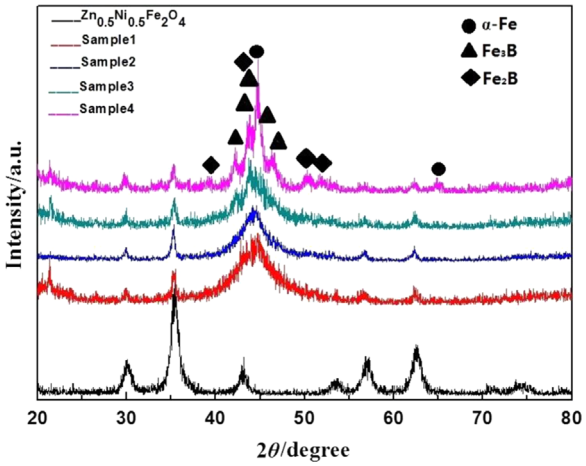

Fig. 1. XRD patterns of $Fe_{76}Si_9B_{10}P_5/Zn_{0.5}Ni_{0.5}Fe_2O_4$ composite prepared by SPS at different sintering temperatures and XRD pattern of $Zn_{0.5}Ni_{0.5}Fe_2O_4$ powders as contrast.

will happen when the sintering temperature is higher than T_x. However, with the above mentioned pressure effect, T_g and T_x will respectively decrease to 477 °C and 527 °C in our study. This means that the sintering temperature to gain amorphous composite under our experimental conditions is 477–527 °C and there will exist severe crystallization in $Fe_{76}Si_9B_{10}P_5$ alloy when the sintering temperature is higher than 527 °C. Nevertheless, there is apparent crystallization when T = 507 °C, which can be attributed to the fact that the pulsing current has a strong influence on the glass transition and crystallization of amorphous alloy during SPS, as it will decrease the T_g and T_x, and consequently promotes the crystallization process [17].

Fig. 2(a) shows the $Fe_{76}Si_9B_{10}P_5$ particles coated by $Zn_{0.5}Ni_{0.5}Fe_2O_4$ nano-particles before sintering. Fig. 2(b) depicts that the sintered sample was dense, and also shows the morphology of micro-cellular structured compacts with cell-body of $Fe_{76}Si_9B_{10}P_5$ particles, and cell-wall of $Zn_{0.5}Ni_{0.5}Fe_2O_4$ particles. It can be observed that the thickness of the cell-wall is 1–2 μm, and the cell-body bonds well with the cell-wall.

Fig.3(a) shows the TEM image of the interface area in the $Fe_{76}Si_9B_{10}P_5/Zn_{0.5}Ni_{0.5}Fe_2O_4$ composite sintered by SPS. It shows that there is a clear interface between area 1 and area 2, and a fusion line between area 2 and area 3. Area 1 is filled up with fine nanoparticles of $Zn_{0.5}Ni_{0.5}Fe_2O_4$ (average particle diameter of 20 nm); area 2 is the fusion zone (50–60 nm) since there are several black grains of α-Fe, and the grain growth has a clear crystal orientation from the fusion line to the internal of area 2; area 3 is $Fe_{76}Si_9B_{10}P_5$ amorphous alloy since there is no obvious imaging contrast. Fig. 3(b) and (d) depict that there is unitary $Zn_{0.5}Ni_{0.5}Fe_2O_4$ phase and $Fe_{76}Si_9B_{10}P_5$ phase in area 1 and area 3, respectively. However, in Fig. 3(c), the EDS results indicate that there are both $Fe_{76}Si_9B_{10}P_5$ phase and $Zn_{0.5}Ni_{0.5}Fe_2O_4$ phase in area 2, and the element contents of Fe, Si, P, Zn, Ni also claim that the main component in area 2 was $Fe_{76}Si_9B_{10}P_5$ alloy with a little of $Zn_{0.5}Ni_{0.5}Fe_2O_4$, so there exists $Zn_{0.5}Ni_{0.5}Fe_2O_4$ particles entering into $Fe_{76}Si_9B_{10}P_5$ matrix.

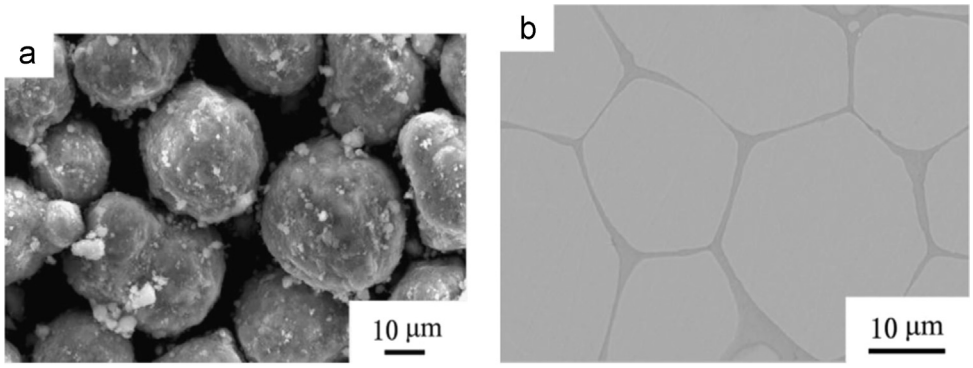

Fig. 2. (a) SEM image of the $Fe_{76}Si_9B_{10}P_5/Zn_{0.5}Ni_{0.5}Fe_2O_4$ composite powders before sintering; (b) SEM image of the composite specimen sintered by SPS (487 °C).

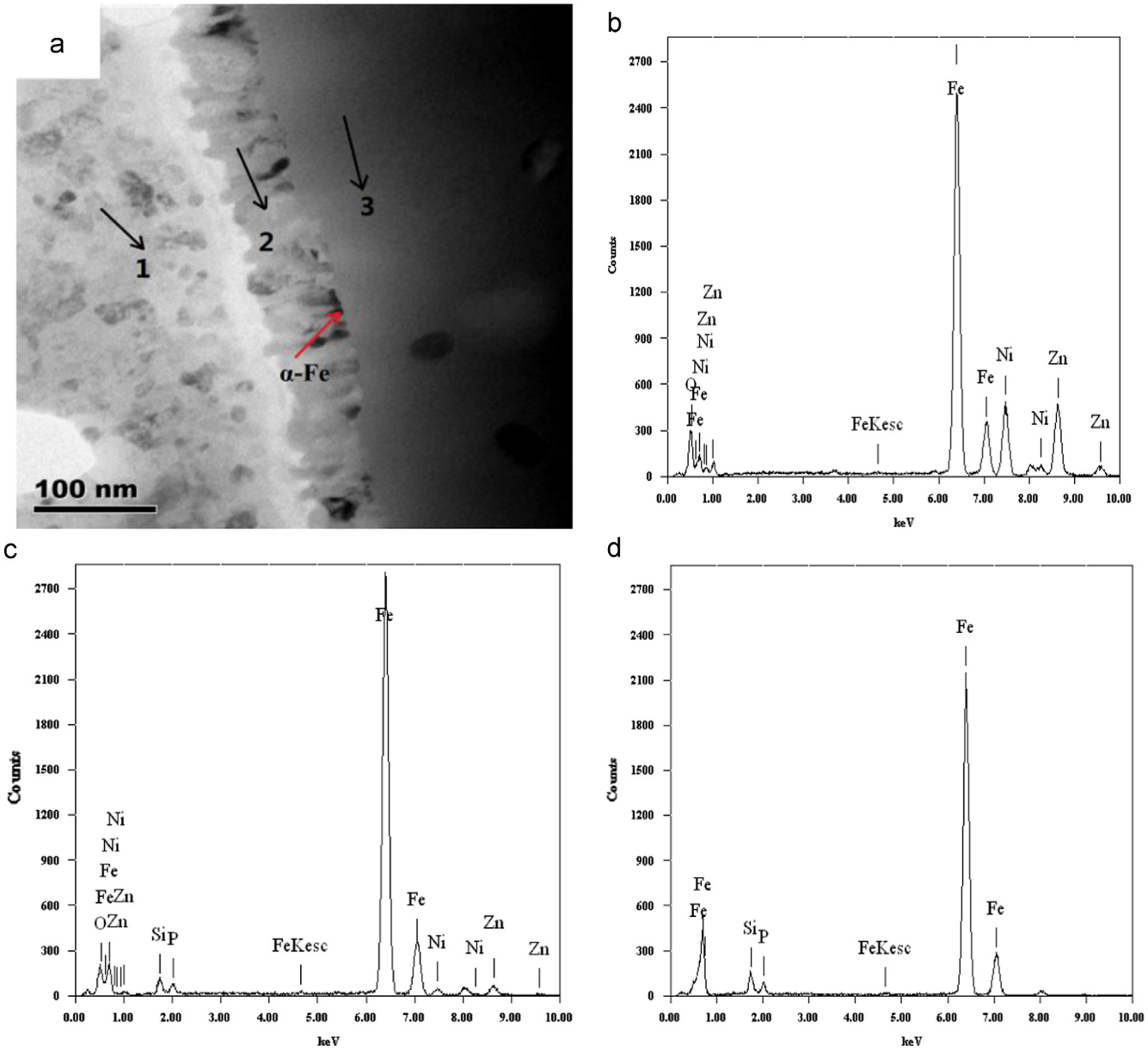

Fig. 3. (a) TEM image of the interface area in the $Fe_{76}Si_9B_{10}P_5/Zn_{0.5}Ni_{0.5}Fe_2O_4$ bulk composite sintered by SPS (487 °C); (b), (c), and (d) the EDS results of area 1,2,3 in Fig. 3 (a), respectively.

According to the abovementioned results, $Fe_{76}Si_9B_{10}P_5$/$Zn_{0.5}Ni_{0.5}Fe_2O_4$ amorphous composite with micro-cellular structure was prepared by SPS at 487 °C, SEM and TEM images showed the homogeneous and dense microstructure of the samples. TEM and EDS results indicated that the temperature and compositions in the interface area are distinct from the core of the particles. Besides, several fine α-Fe particles were observed by TEM, and the grain growth had a clear crystal orientation. Since the crystallization was slight and local, the XRD pattern of sample 2 in Fig. 1 still presented an amorphous state for the whole.

4. Discussion about the sintering mechanism

The theoretical sintering temperature of $Zn_{0.5}Ni_{0.5}Fe_2O_4$ is about 1000–1200 °C [18], but our sintering temperature is set on the basis of the sintering temperature of $Fe_{76}Si_9B_{10}P_5$ amorphous alloy as 487 °C. The difference between the macroscopic temperature and theoretical sintering temperature indicates an inhomogeneous temperature distribution in the sample. We consider that the instantaneous high temperature comes from the internal heat source in the sample. The "macroscopic low temperature sintering" phenomenon of $Zn_{0.5}Ni_{0.5}Fe_2O_4$ nano-particles is a meaningful question for further study, and will give the help to investigate the sintering mechanism of $Fe_{76}Si_9B_{10}P_5$/$Zn_{0.5}Ni_{0.5}Fe_2O_4$ composite.

It has been reported in previous studies that the sintering mechanism of SPS process is different for conductive and nonconductive materials. (1) conductive materials: the pulse current mainly flows through the sample, and the gaps between particles make it possible to stimulate plasmas and discharging at the initial stage of sintering, and there will generate numerous Joule heat and discharging heat to form "instantaneous local high temperature" (formed mainly because of the heat generated with the contact resistance) at the particles surfaces [6,19]. (2) non-conductive materials: the pulse current would always choose the path with the least resistance [20], so it mainly flows through the conducting punches and the die [1,21], and there will generate Joule heat for their intrinsic resistance. The powders are then heated by the heat conduction from the die and the punches, so there will be an inhomogeneous thermal gradient from the inside surface of the die to the sintered particles. However, the internal particles of $Fe_{76}Si_9B_{10}P_5$ alloy are conductive material while the $Zn_{0.5}Ni_{0.5}Fe_2O_4$ outer film is poorly-conductive or even as non-conductive, since its resistance is 10^4 Ω m [18]. Since the resistance of $Fe_{76}Si_9B_{10}P_5$/$Zn_{0.5}Ni_{0.5}Fe_2O_4$ powders is 10 Ω m, the pulse current cannot flow through the powders, mainly through the die. The die is the heat source for nonconductive material. It is difficult to achieve excellent sintering of $Zn_{0.5}Ni_{0.5}Fe_2O_4$ particles and just relies on the heat conduction of the die. Thus the above mentioned mechanisms do not apply to our study.

In this experiment, the $Zn_{0.5}Ni_{0.5}Fe_2O_4$ outer film is poorly conductive of 1–2 μm thick, which is very thin and small enough to lead the sparks pass through, and will trigger spark discharging and spark plasmas under SPS conditions (specific pressure, pulsing current and electromagnetic field) [15]. With the electric field effect, there will create tip effect since the curvature radius of $Zn_{0.5}Ni_{0.5}Fe_2O_4$ nanoparticles is small, which is easy to form strong electric field and then cause the rarefied gases between $Zn_{0.5}Ni_{0.5}Fe_2O_4$ nanoparticles ionized, and to create plasmas. The local discharging is promoted in this process. Furthermore, the positive ions and electrons created in ionization process are accelerated by the electric field, and collide with the atoms during the movement to form collision ionization, which will create more plasmas. The process continues in this way, and it will stimulate positive ions and electrons increasing with an "avalanche mode", and thus greatly promotes the discharging process and the plasmas creation. Heated by the energy generated by local discharging, the surface temperature of $Zn_{0.5}Ni_{0.5}Fe_2O_4$ particles will increase greatly during a very short period, therefore to form instantaneous local high temperature in $Zn_{0.5}Ni_{0.5}Fe_2O_4$ area, which may be higher than the theoretical sintering temperature of $Zn_{0.5}Ni_{0.5}Fe_2O_4$ particles. Thus the local sintering and densification of $Zn_{0.5}Ni_{0.5}Fe_2O_4$ particles are complete with the applied pressure. Simultaneously, the local high temperature will stimulate the adjacent gaps discharging, thus facilitate the continuous formation of new discharging path in a self-propagating mode. Finally, sintering and densification of the whole sample is complete. Such process effectively achieves excellent "macroscopic low temperature sintering" of $Fe_{76}Si_9B_{10}P_5$/$Zn_{0.5}Ni_{0.5}Fe_2O_4$ amorphous composite. According to the abovementioned discussion, the schematic diagram of the instantaneous local high temperature distribution from the surface of the $Fe_{76}Si_9B_{10}P_5$ amorphous alloy to the core can be seen in Fig. 4. It shows that there is a high temperature zone in the $Zn_{0.5}Ni_{0.5}Fe_2O_4$ area. It forms a great thermal gradient in a very short time from the $Zn_{0.5}Ni_{0.5}Fe_2O_4$ area to the $Fe_{76}Si_9B_{10}P_5$ alloy. It must be noted that the heating rate will increase greatly in a very short time since the local high temperature is instantaneous. T_x and T_g will increase significantly when increasing the heating rate [22], so the crystallization zone becomes narrow and is not legible in Fig. 3(a). According to the characteristics of heterogeneous nucleation

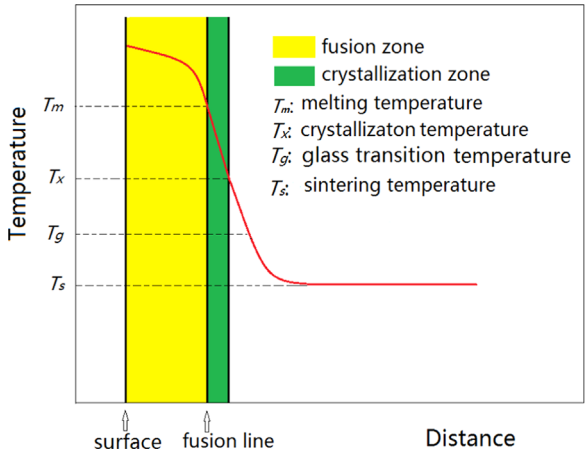

Fig. 4. Schematic diagram of the instantaneous local high temperature distribution from the surface of the $Fe_{76}Si_9B_{10}P_5$ amorphous alloy to the core, formed by the effect of plasmas discharging.

[23], as a result of the crystallization zone is narrow and close to the fusion zone, it can provide initial heterogeneous nucleation place of α-Fe. The grains formed by the crystallization become the solidification cores of the fusion zone.

However, the temperature measuring point of SPS is on the die cavity surface, so the measuring data was just the macroscopic temperature of a point, it could not represent the local and microcosmic high temperature.

5. Conclusions

The bulk amorphous composite with micro-cellular structure has been prepared by SPS with the cell-body of $Fe_{76}Si_9B_{10}P_5$ particles and cell-wall of $Zn_{0.5}Ni_{0.5}Fe_2O_4$ particles at a low sintering temperature of 487 °C.

The mechanism of SPS process for $Fe_{76}Si_9B_{10}P_5/Zn_{0.5}Ni_{0.5}Fe_2O_4$ composite is the instantaneous local high temperature formed by the creation of plasmas and the self-propagating mode of the formation of new discharging path. The tip effect of $Zn_{0.5}Ni_{0.5}Fe_2O_4$ nanoparticles promotes the local discharging in the gaps, and with the effect of electric field, collision ionization greatly facilitates the discharging process and plasmas creation. Discharging energy forms an instantaneous local high temperature to complete the local sintering and densification of $Zn_{0.5}Ni_{0.5}Fe_2O_4$ particles with the applied pressure. Simultaneously, the local high temperature will stimulate the adjacent gaps discharging, thus facilitate the continuous formation of new discharging path. Finally, the sintering and densification of the whole sample is complete.

Acknowledgments

The authors would like to acknowledge the National Natural Science Foundation of China (51071034) and Natural Science Foundation of Jilin Province (No. 20150101021JC) for the financial supported.

References

[1] Z.K. Zhao, C.T. Chang, A. Makino, A. Okubo, A. Inoue, Mater. Trans. 50 (2009) 487–489.
[2] A. Inoue, Acta Mater. 48 (2000) 279–306.
[3] A. Makino, T. Kubota, C.T. Chang, M. Makabe, A. Inoue, Mater. Trans. 48 (2007) 3024–3027.
[4] A. Makino, T. Kubota, M. Makabe, C.T. Chang, A. Inoue, Mater. Sci. Eng. B148 (2008) 166–170.
[5] A. Inoue, Mater Trans. 36 (1995) 866–875.
[6] Z.A. Munir, U. Anselmi-Tamburini, J Mater Sci. 41 (2006) 763–777.
[7] G.Q. Xie, F.X. Qin, S.L. Zhu, A. Inoue, Intermetallics 29 (2012) 99–103.
[8] G.Q. Xie, M. Fukuhara, D.V. Louzguine-Luzgin, A. Inoue, Intermetallics 18 (2010) 2014–2018.
[9] S.M. Lee, H. Kato, T. Kubota, A. Makino, A. Inoue, Intermetallics 17 (2009) 218–221.
[10] D. Roy, S. Kumari, R. Mitra, I. Manna, Intermetallics 15 (2007) 1595–1605.
[11] S.W. Wang, Y.S. Kang, M. Niino, T. Hirai, Mater. Res. Bull. 35 (2000) 619–628.
[12] S.W. Wang, Y.S. Kang, M. Niino, T. Hirai, J. Mater. Res. 15 (2000) 982–987.
[13] Y.C. Wang, Z.Y. Fu, Q.J. Zhang, Key Eng. Mater. 224 (2002) 717–720.
[14] X.Y. Song, X.M. Liu, J.X. Zhang, J. Am. Ceram. Soc. 89 (2006) 494–500.
[15] Z.K. Zhao, K.F. Yao, J.F. Li, Chin Sci Bull. 51 (2006) 235–239.
[16] F. Ye, K. Lu, Acta Mater. 47 (1999) 2449–2454.
[17] W.F. Wu, K.F. Yao, Z.K. Zhao, Chin. Sci. Bull. 49 (2004) 2581–2585.
[18] A. Costa, E. Tortella, M.R. Morelli, R. Kiminami, J. Magn. Magn. Mater. 256 (2003) 174–182.
[19] R. Raj, J. Eur. Ceram. Soc. 32 (2012) 2293–2301.
[20] S.B. Sinnott, E.C. Dickey, Mater. Sci. Eng. R43 (2003) 1–59.
[21] R. Chaim, J. Mater. Sci. 48 (2013) 502–510.
[22] A. Inoue, T. Zhang, N. Nishiyama, K. Ohba, Mater. Trans. JIM 34 (1993) 1234–1237.
[23] Y.W. Lin, K.L. Lin, Intermetallics 32 (2013) 6–11.